RSC Advances

ROYAL SOCIETY OF CHEMISTRY

www.rsc.org/advances

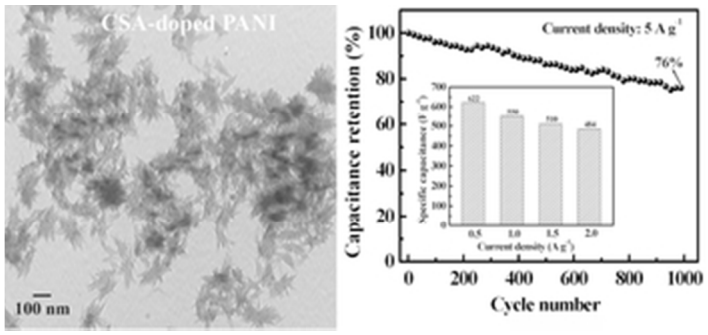

29x13mm (300 x 300 DPI)

Block copolymer–guided fabrication of shuttle–like polyaniline nanoflowers with radiated whiskers for application in supercapacitors

Hongyu Mi,[*a] Jiapan Zhou,[a] Zongbin Zhao,[b] Chang Yu,[b] Xuzhen Wang[b] and Jieshan Qiu[*b]

[a]Xinjiang Laboratory of Advanced Functional Materials, School of Chemistry and Chemical Engineering, Xinjiang University, Urumqi 830046, China

[b]Carbon Research Laboratory, School of Chemical Engineering, State Key Lab of Fine Chemicals, Dalian University of Technology, Dalian 116023, China

* Corresponding author. Fax: +86 991 8582809, Fax: +86 411 84986072.

E-mail address: mmihongyu@163.com; jqiu@dlut.edu.cn.

Superfine shuttle–shaped polyaniline (PANI) nanoflowers with radiated whiskers in the edge of flowers have been synthesized in block copolymer–assisted reverse microemulsion system. The copolymer poly(ethylene oxide)–block–poly(propylene oxide)–block–poly(ethylene oxide) (P123) served as the surfactant stabilizing reverse micelles for regular assembly of flower–like structures. The flowers formed had widths of ca. 40−150 nm and lengths of ca. 80−180 nm, far less than typical sizes reported (over several microns). The correlation between some important factors (polymerization method, P123 and aniline concentrations and reaction time) and morphologies was discussed, and a plausible mechanism forming nanoflowers was put forward. More importantly, the unique architecture showed good electrochemical properties with high reversible capacitance (622 F g^{-1} at 0.5 A g^{-1}, and 484 F g^{-1} at 2 A g^{-1}) and good durability (76% capacitance retention at 5 A g^{-1} after 1000 cycles) due to nano size and V–typed channels. These characteristics make it promising in supercapacitor applications.

1. Introduction

Owing to its promising prospects in the areas of supercapacitors, batteries, chemical sensors, corrosion protection and drug delivery, polyaniline (PANI) as one of popular conductive polymers, has aroused lots of attention.[1–3] Under increasingly serious resources and environment problems, PANI especially nanostructured PANI, is more often studied as supercapacitor electrode materials, and achieves electrochemical properties superior to their bulk counterparts owing to nano–size effect that offer larger electrode-electrolyte interfaces, shorter ion/electron transport lengths, faster electrochemical response and better strain buffering.[4–6] Hence, much effort has focused on the fabrication and assembly of nano–sized PANI with controllable doped structure and morphology. Thus far, diverse microstructures ranging from one-dimensional (1D) tubes/wires/fibers/rods/belts,[7–15] two–dimensional (2D) plates/film/rings[16–19] to three–dimensional (3D) flowers[20–25] have been made. Of those, 1D PANI was frequently synthesized by many approaches such as conversional chemical oxidation method, interfacial polymerization method, soft/hard templating method, microemulsion method and electrochemical method, and showed enhanced electrochemical properties. For instance, Alshareef et al.[8] assembled full–cell pseudocapacitors based on PANI nanotubes obtained by reactive oxide templating method, which delivered a remarkable energy density of 84 W h kg^{-1} and a power density of 182 kW kg^{-1}. Sk et al.[26] synthesized heparin–controlled porous PANI nanofibers networks using chemical oxidation method, which showed a capacitance of about 732.18 F g^{-1} at 1 mA and long cycle life (72.28% retention after 1000 cycles). Mallouk and the coworkers[27] fabricated a template grown PANI, and it showed a capacitance of 700 F g^{-1} at a current density of 5 A g^{-1}. More recently, Qin et al.[28] achieved core–shell PANI/PPy by in situ chemical polymerization and further seed polymerization, which exhibited 346 F g^{-1} at a scan rate of 5 mV s^{-1}. However, the approach to

3D PANI is the least reported, and mainly concentrates on chemical oxidation routes in the presence of various additives.[20,23–25] Besides, the studies concerning the electrochemical performance of 3D PANI are scare despite possibly achieving remarkable properties significantly benefited from their multidimensional structure.[20]

Poly(ethylene oxide)–block–poly(propylene oxide)–block–poly(ethylene oxide) (P123), an amphiphilic triblock copolymer, popularly acts as the template guiding the formation of mesoporous silicates[29,30] and other inorganic nanomaterials[31–34]. There are to our knowledge few literatures involving block copolymer–assisted synthesis of 3D PANI. For instance, in the work of Guo et al.,[16] block copolymer F127 template in aqueous system was used to fabricate leaf-structured PANI. Srivastava et al.[35] synthesized a mesostructured PANI by templating approach using mixed surfactants of anionic sodium dodecylsulfate and non–ionic block copolymer P123 in a aqueous system. However, there are no reports on the combination of block copolymer–templated strategy with reverse microemulsion polymerization method for fabricating 3D nanostructured PANI. The advantage of this approach is that it can achieve strict control over PANI growth in a confined microenvironment derived from surfactant micelles within oil phase, thus providing a simple and effective way for the synthesis of 3D PANI with very small size. Besides, owing to rich phase behavior of block copolymer,[36] the block copolymer–guided method can provide an alternative route to synthesize 3D PANI superstructures in a stable water–in–oil (W/O) system, which may be applicable to ordered assembly of other nanomaterials. Based on the above analysis, in this work, we present an original method to prepare flower–shaped PANI multidimensional superstructures using P123–based micelles as the template in W/O system for the first time. Some important factors that influence the morphology and size of PANI are explored, and a possible mechanism for flower growth is proposed. Especially,

electrochemical performance of PANI nanoflowers are investigated and compared with that of well–developed PANI nanofibers in order to verify the potential of PANI nanoflowers as electrode materials in supercapacitors.

2. Experimental

2.1 Materials

Poly(ethylene oxide)–block–poly(propylene oxide)–block–poly(ethylene oxide) (denoted as P123 or $PEO_{20}PPO_{70}PEO_{20}$, MW = 5800) was purchased from Sigma Aldrich. Camphor sulfonic acid (CSA) was received from J&K Scientific Ltd. Aniline (AN) was purified by distillation before use. All other chemicals and solvents were purchased from commercial suppliers, which were analytically graded and used as received.

2.2 Synthesis of PANI nanoflowers

Two reverse microemulsion systems (RMS1 and RMS2) were firstly prepared. Generally, P123 (0.25 mmol) and CSA (20 mmol) was dissolved in deionized water (15 mL) with vigorously stirring for 30 min, followed by the addition of hexane (25 mL) and n–hexanol (4.5 mL). After stirring for 30 min, AN (5.5 mmol) was added and continue to magnetically stir for 2 h at ice–water bath, forming RMS1. The concentrations of P123 and AN in RMS1 were about 0.006 M and 0.12 M, respectively. RMS2 was prepared under parallel conditions with APS (5 mmol) instead of AN. Next, RMS2 was slowly added to RMS1 under stirring in ice–water bath, and the resultant solution was left undisturbed for 24 h at 8~10 °C. Finally, the dark green PANI was obtained by centrifuging–rinsing repeatedly and freeze–drying. For investigating the effect of some reaction factors on the PANI morphology, various PANI samples were prepared by varying the type of the surfactant and the concentrations of P123 and AN following the above procedure.

2.3 Material characterization

Transmission electron microscopy (TEM) micrographs of samples were obtained with a HITACHI–600 transmission electron microscope. Infrared (IR) spectrum in the range 400–4000 cm^{-1} was taken with a BRUKER-EQUINOX–55 infrared spectrometer using KBr pellets. X–ray diffraction (XRD) pattern was recorded on a BRUKER D8 Advance powder diffractometer with a Cu K target ranging from 5 to 80 °C. The surface area of the sample was examined by Brunauer–Emmett–Teller (BET) measurement on an automatic ASAP 2020 analyzer.

2.4 Electrochemical measurement

The working electrode (~0.5 cm^2) composed of 80 wt.% PANI, 10 wt.% acetylene black and 10 wt.% polytetrafluorethylene (the loading of PANI in the electrode was 2.4 mg cm^{-2}) using carbon paper as current collector was immersed in 1M H_2SO_4 electrolyte overnight and taken for electrochemical tests on CHI660C electrochemical workstation and a CT2001A Land Battery Testing System in a classical three–electrode mode at room temperature. The reference electrode was saturated calomel electrode (SCE), and the counter electrode was Pt electrode. Cyclic voltammetry (CV), galvanostatic charge/discharge (CD) tests were performed in a sweep potential ranging from –0.2 V to 0.8 V. The specific capacitance (C_m) can be calculated by CD curves using the equation: $C_m = (I\Delta t/m\Delta V)$, where I is the discharge current (mA), Δt is the discharge or charge time (s), ΔV is the potential window and m is the weight of active material in electrode (mg). Electrochemical impedance spectroscopy (EIS) test was carried out in a frequency range from 10^4 to 0.01 Hz.

3. Results and discussion

3.1 Morphology

Typical TEM micrographs of PANI products made from reverse and conventional microemulsion polymerization methods are presented in Fig. 1. It is found that both synthetic

approach and the type of the surfactant noticeably affect the morphology of the products. As revealed in Fig. 1a, PANI synthesized by P123–assisted reverse microemulsion polymerization consists of small shuttle–shaped flower–like nanostructures with widths of ca. 40−150 nm and lengths of ca. 80−180 nm. Its shape and size are significantly different from results reported.[20,21] For instance, the spherical flowers described by Alshareef et al.[8], Guo et al.[20] and Wang et al.[21] are around 3 μm, 4.5 μm and 10−20 μm in size, respectively. Further careful observation finds that the edges of flowers have some radiated whiskers, constructing rich V–typed channels on surfaces. When P123 is replaced by CTAB without changing other conditions (Fig. 1b), well dispersed short nanofibers rather than nanoflowers appear in the product. Their diameters and lengths are estimated to be ca. 20−30 nm and ca. 100−200 nm, respectively, which are very small compared to the previous reports.[11,26,37–39] With conventional microemulsion method in the presence of P123 (Fig. 1c), the as–prepared PANI is still short nanofibers. Compared with those from the above case, although fibers so fabricated have a smaller size (ca. 15−30 nm diameter and ca. 50−100 nm length), their dispersity is not very good. TEM results manifest that micelle templating approach readily yields PANI with small size, and P123–stabilized reverse microemulsion route has the ability to generate special flower−structured PANI.

Fig. 2 depicts TEM images of PANI obtained with P123 concentration ranging from 0 M to 0.011 M. Apparently, the concentration of P123 has significant effect on the morphology of the products. In the absence of P123 (Fig. 2a), PANI has irregular fiber–like structures with diameters and lengths of ca. 30−70 nm and ca. 80−250 nm, respectively. In this case, PANI nanofibers are actually synthesized in an immiscible aqueous/organic bi–phase system by interfacial polymerization. This result verifies again that interfacial polymerization method is an effective and simple strategy to fabricate fibrous morphology. At low P123 concentration of

0.002 M (Fig. 2b), some flower–like aggregates appear, but few fiber–like structures still exist. When P123 concentration is increased to 0.006 M, PANI is shuttle–like nanoflowers (Fig. 2c). At a higher concentration (0.011 M) (Fig. 2d), flower shape still remain, but its size slightly decreases possibly because excessive adsorption of P123 on the surfaces of PANI nuclei limits their further growth.[31] The above results indicate that, with P123 concentration increasing from 0 to 0.011 M, the morphology of PANI varies from nanofibers to nanoflowers, accompanying with the slight decrease of the size of nanoflowers. Considering that the removal of the surfactant with high concentration in the system is very time–consuming to purify the product as much as possible, therefore, P123 concentration of 0.006 M was regarded as a proper condition for the preparation of flower–shaped PANI.

Fig. 3 shows TEM images of PANI synthesized with AN concentration ranging from 0.07 M to 0.17 M. At low concentration of AN (0.07 M), some irregular particles close to flower shape start to form with detectable short whiskers on the edge of flowers (Fig. 3a). As AN concentration increases to 0.12 M (Fig. 1a and 2c), the product exhibits well–defined flower structures with pronounced whiskers. With the AN concentration up to 0.17 M, one can only see short fibers instead of flowers, which may be caused by high reaction rate that is not beneficial to the assembly of fibers. These fibers have very coarse surfaces, with diameters of ca. 40−70 nm. The above morphology investigation well reveals that, with the increase of AN concentration, the as–obtained PANI is inclined to form fibrous structures. The possible reason for this is that high monomer (AN) concentration leads to high reaction rate, which may not be beneficial to the assembly of fibers into nanoflowers.

The images of PANI obtained from various polymerization stages are displayed in Fig. 4, which experimentally indicates the evolution process of PANI from 1D nanofibers to 3D

nanoflowers. At the initial stage of the polymerization (about 10 min) (Fig. 4a), nanofibers with ca. 10−20 nm diameter are a dominating morphology of PANI. After the reaction for 30 min, most of nanofibers are converted to nanoflowers, leading to coexisting morphologies of a large majority of nanoflowers and few nanofibers in the products (Fig. 4b). As the reaction time increases to 1 h, almost all PANI samples exhibit nanoflower morphology but a part of nanoflowers is still in an incomplete growth state (Fig. 4c). As the reaction proceeds for 5 h (Fig. 4d), PANI shows a uniform flower shape. After the reaction of 24 h, well–grown PANI nanoflowers with more abundant whiskers on surfaces are successfully achieved.

3.2 Formation mechanism

On the basis of the above results and previous studies on block copolymer-assisted organic/inorganic nanomaterials,[20,31,33] the fabrication process and possible mechanism for the evolution from randomly oriented nanofibers to higher order nanoflowers are depicted in Fig. 5. Step 1, the formation of stable hexane/n–hexanol/water/P123/AN system (RMS1). From the molecular structure presented, it clearly shows that P123 is an amphiphilic molecule consisting of hydrophilic (PEO) block and hydrophobic (PPO) block. The introduction of P123 into deionized water easily leads to the generation of P123 micelles with hydrated PEO corona and PPO core at the micelle surface.[40,41] As large amount of organic solvents is mixed with P123 micelles, these micelles are dispersedly confined within oil phase by the barrier role of P123 surfactant located on water/oil interfaces. Here, a confined aqueous microenvironment derived from P123 micelles readily allows the nucleation, growth and further assembly of PANI.[29] With the introduction of AN into this W/O system for further stirring for 2 h, RMS1 forms with AN adsorbed on P123 chains through electrostatic attraction. Step 2, the polymerization of AN. When the hexane/n–hexanol/water/P123/APS system (RMS2) is added dropwise into RMS1, AN

is firstly polymerized at oil–water interface and then grows towards water phase. Initially, randomly oriented short fibers are formed, and then these fibers act as nucleation sites for subsequent assembly of ordered nanoflowers through the intra–/inter–molecular interaction between the fibers.[25] The above analysis illustrates that P123–stabilized reverse micelles can serve as the microreactor and template for constructing flower-based superstructures. Such 3D nanoscale architectures with open V–typed channels on surfaces can greatly boost the immigration of electrolyte ions into the interior of active materials through these channels. Therefore, one can predict that the as–formed PANI may possess favorable electrochemical characteristics.

3.3 Chemical structure

The chemical structure of the resultant PANI nanoflowers is examined by IR spectrum, as shown in Fig. 6a. Some typical bands can be clearly seen at 1563, 1480, 1290, 1131, 1044, 784 and 581 cm^{-1}. They respectively correspond to C=C stretching of quinoid ring, C=C stretching of benzenoid, C–N stretching of secondary aromatic amine, N=Q=N stretching (Q represents quinoid ring), S=O stretching, C–H out–of–plane bending vibration, and S–O stretching, indicating the formation of CAS–doped PANI. Generally, PANI has several forms, i.e. leucoemeraldine base (fully reduced form), emeraldine base (half–oxidized form), and pernigraniline base (fully oxidized form). When the intensity ratio (R) of quinoid–to–benzenoid is 1, PANI is in conductive emeralding salt state. In Fig. 6a, R value of 0.91 verifies that PANI obtained is close to conducting emeraldine salt fashion and is identical to the previous report.[35] Crystalline structure of the product is examined by XRD pattern. Different from amorphous PANI with relatively plane pattern, the nanoflowers show three pronounced diffraction peaks (Fig. 6b), such as (15.4^o), (20.5^o) and (25.5^o). They represent the repeat unit of PANI chain, the

periodicity parallel and perpendicular to the polymer chain, respectively, indicating that PANI nanoflowers have a crystalline structure. Its crystalline degree is estimated to be about 0.48 based on integral intensities of the radiations diffracted by crystalline (I_c) and amorphous (I_a) phases: $W_{cr} = I_c/(I_a + I_c)$.[42] Generally, PANI with an order structure favors a rapid charge/discharge process by providing a high conductivity pathway,[43] and thus PANI nanoflowers obtained may show the improved electrochemical performance. Finally, N_2 adsorption−desorption isotherms and corresponding pore size distribution of PANI nanoflowers are presented in Fig. 6c. IV−typed isotherms with a hysteresis loop indicate porous characteristic of PANI nanoflowers. The specific surface area of PANI nanoflowers is calculated to be about 30 $m^2\ g^{-1}$.

3.4 Electrochemical performance

As far as we know, it is well established that many 1D nano–structured PANI samples exhibit good capacitive performance due to nano–size effect and high doping level.[8,9,11,13,26–28, 39,44–46] Among various PANI nanofibers obtained in this study, PANI nanofibers prepared using CTAB instead of P123 possess uniform morphology and very small size, which may deliver good performance. Thus, to verify that PANI nanoflowers obtained can also perform well electrochemically, PANI nanoflowers and nanofibers are subjected to test cyclic voltammetry (CV) and galvanostatic charge/discharge (CD) in a classical three–electrode cell, and the results are compared and summarized in Fig. 7. Firstly, rate–dependent CV tests of two electrodes are made in 1 M H_2SO_4 solution over a range of 1 to 9 mV s^{-1}. As shown in Fig. 7a and 7b, several couples of anodic and cathodic redox peaks can be observed in all CV curves, manifesting that their charge storage mode follows Faradaic redox mechanism. The peak pairs in O1/R1 and O3/R3 are ascribed to the leucoemeraldine–polaronic emeraldine redox transition, while the O2/R2 and O4/R4 peak pairs come from the emeraldine–pernigraniline transformation.[13,47]

Notably, with scan rate increasing, the cathodic and anodic peaks for two electrodes slightly shift positively and negatively, respectively, which is mainly caused by the resistance of the electrode. Besides, the fact that redox peak currents increase with the increase in scan rate confirms fast current response of PANI nanoflowers and nanofibers.

Galvanostatic CD curves of PANI nanoflowers and nanofibers at current densities of 0.5, 1, 1.5 and 2 A g^{-1} are presented to determine their specific capacitance (C_m) values, as shown in Fig. 7c and 7d. A near symmetric feature of charge/discharge curves at high current density suggests that two electrodes have good electrochemical reversibility. Charge and discharge capacitances of PANI nanoflowers are calculated to be 1010 and 622 F g^{-1} at a current density of 0.5 A g^{-1}, respectively, which are slightly lower than those of PANI nanofibers (1155 and 705 F g^{-1}). Further, the theoretical capacitance of PANI nanoflowers is also calculated for comparison. According to the equation:[26,48] $C_{max} = \alpha F/\mathrm{d}VM + C_{dl}A$, where α, F, $\mathrm{d}V$, M, C_{dl} and A are the fraction of electron shared on each monomer unit (the maximum value of α is 1 in PANI), the Faraday constant (96485.3 C mol^{-1}), the potential range (V), the molecular weight of aniline (91.1 g mol^{-1}), the double layer capacitance (about 30 μF cm^{-2})[48] and the specific surface area (m^2 g^{-1}), respectively. Based on the specific surface area of PANI nanoflowers (30 m^2 g^{-1}), its theoretical C_{max} is calculated to be about 1068 F g^{-1}. Therefore, the discharge capacitance of PANI nanoflowers (622 F g^{-1} at 0. 5 A g^{-1}) can deliver about 58% of its theoretical value due to low α value. Although the use of very low current density can lead to significantly high C_m close to its theoretical value, this strategy is not advocated because low current is unsuitable for high power applications in supercapacitors.[26]

The specific capacitance–current profiles of two electrodes are inserted in Fig. 7c and 7d, respectively. With the increase of current density, their C_m values have a decrease caused by

internal resistance. In spite of this, PANI nanoflowers still remain charge and discharge capacitances of 510 and 484 F g^{-1} even at a rate of 2 A g^{-1}. Although the C_m values of PANI nanoflowers are somewhat lower than those of PANI nanofibers (634 and 578 F g^{-1} at 2 A g^{-1}), their capacitance retention is comparable (78% for nanoflowers and 82% for nanofibers). This confirms that both PANI electrodes have the ability to yield high capacitance at high current density. On the other hand, the C_m values of PANI nanoflowers are also superior to those from crosslinked PANI nanorods (297 F g^{-1} at 1 A g^{-1}),[13] PANI nanofibers (192 F g^{-1} at 0.1 A g^{-1})[40], and PANI nanofibers (548 F g^{-1} at 0.18 A g^{-1})[41]. These data can well illustrate that PANI nanoflowers and nanofibers have high specific capacitance and good rate performance. High performance may be ascribed to more and shorter diffusion paths of ions and electrons, highly accessible specific surface area and good electrical conductivity brought by 1D or 3D nano–sized structure of doped PANI.

The cycling properties of PANI nanoflowers and nanofibers are measured by charge–discharge cycling at a current density of 5 A g^{-1}. As shown in Fig. 7e, PANI nanoflowers can retain about 76% of initial capacitance at high current density of 5 A g^{-1} after 1000 charge/discharge cycles, which is higher than that of PANI nanofibers (69%), demonstrating that PANI nanoflowers exhibit better electrochemical stability due to its multidimensional superstructures with nano size and V–typed channels.

The Nyquist plots of PANI nanoflowers and nanofibers are depicted in Fig. 7f. Two electrodes show similar impedance characteristics. At low frequency, two straight lines are nearly parallel to the imaginary axis, confirming good capacitive behavior. At high frequency, one can estimate from the enlarged plots in the inset of Fig. 7f that charge–transfer resistance (R_{ct}) values of PANI nanoflowers and nanofibers are around 1.3 and 1.4 Ω based on the diameter of the semicircle,

and their internal resistance (R_s) values are about 1.9 and 1.5 Ω based on the high frequency intercept of the real axis. Small R_{ct} and R_s values indicate that two electrodes have low charge–transfer resistance and ion diffusion resistance during electrochemical charge/discharge process, which has the contribution to high–performance electrochemical behavior.

4. Conclusions

P123–assisted reverse microemulsion method has been demonstrated to be effective for tailoring PANI architectures from 1D fiber to 3D flower. Reverse P123 micelles play important roles in controlling flower growth. The novelty of the present work mainly has two points. Firstly, through the exploration on the formation mechanism of nanoflowers, one can clearly understand the formation of shuttle–like PANI nanoflowers obtained from an original approach. This will provide some inspiration for designing other interesting multidimensional structures. Secondly, particular emphasis is placed on the capacitive properties of such PANI flowers for the first time. The results demonstrate that the electrochemical performance of PANI nanoflowers is comparable to that of well–developed PANI nanofibers, exhibiting high specific capacitance, good rate capability and good cycling stability due to nanoscale size, open V–shaped channels and high doping level. Therefore, PANI nanoflowers obtained may be a promising candidate for energy storage applications.

Acknowledgements

This work is supported by the Scientific Research Program of the Higher Education Institution of XinJiang (No. XJEDU2012I05), the National Natural Science Foundation of China (No. 21363023, and No. U1203292), and the Open Project Program of Xinjiang Laboratory Advanced Functional Materials, China (XJDX0902-2012-05).

References

1 K. Lee, S. Cho, S. H. Park, A. J. Heeger, C. W. Lee and S. H. Lee, *Nature*, 2006, **441**, 65–68.

2 C. Li, H. Bai and G. Shi, *Chem. Soc. Rev.*, 2009, **38**, 2397–2409.

3 J. F. Mike, L. Shao, J. W. Jeon and J. L. Lutkenhaus, *Macromolecules*, 2014, **47**, 79–88.

4 A. N. Aleshin, *Adv. Mater.*, 2006, **18**, 17–27.

5 G. P. Hao, F. Hippauf, M. Oschatz, F. M. Wisser, A. Leifert, W. Nickel, N. Mohamed-Noriega, Z. Zheng and S. kaskel, *ACS Nano*, 2014, **8**, 7138–7146.

6 M. A. Bavio, G. Acosta and T. Kessler, *J. Power Sources*, 2014, **245**, 475–481.

7 J. X. Huang, S. N. Virji, B. H. Weiller and R. B. Kaner, *J. Am. Chem. Soc.*, 2003, **125**, 314–315.

8 W. Chen, R. B. Rakhi and H. N. Alshareef, *J. Mater. Chem. A,* 2013, **1**, 3315–3324.

9 J. Mu, G. Ma, H. Peng, J. Li, K. Sun and Z. Lei, *J. Power Sources*, 2013, **242**, 797–802.

10 Z. D. Zujovic, C. Laslau, G. A. Bowmaker, P. A. Kilmartin, A. L. Webber, S. P. Brown and J. Travas-Sejdic, *Macromolecules*, 2010, **43**, 662–670.

11 K. Wang, J. Huang and Z. Wei, *J. Phys. Chem. C,* 2010, **114**, 8062–8067.

12 Y. Liao, V. Strong, W. Chian, X. Wang, X. G. Li and R. B. Kaner, *Macromolecules*, 2012, **45**, 1570–1579.

13 X. Wang, J. Deng, X. Duan, D. Liu, J. Guo and P. Liu, *J. Mater. Chem. A*, 2014, **2**, 12323–12329.

14 P. Anilkumar and M. Jayakannan, *Macromolecules*, 2008, **41**, 7706–7715.

15 G. R. Li, Z. P. Feng, J. H. Zhong, Z. L. Wang and Y. X. Tong, *Macromolecules*, 2010, **43**, 2178–2183.

16 J. Han, G. Song and R. Guo, *Adv. Mater.*, 2007, **19**, 2993–2999.

17 H. Fan, H. Wang, J. Guo, N. Zhao and J. Xu, *J. Colloid Interf. Sci.*, 2013, **409**, 255–258.

18 S. Y. Shen, Y. J. Wu, K. S. Ho, T. H. Hsieh, T. H. Ho, Y. Z. Wang, P. H. Tseng and Y. C. Hsu, *Polymer*, 2011, **52**, 2609–2617.

19 G. Li, Y. Li, Y. Li, H. Peng and K. Chen, *Macromolecules*, 2011, **44**, 9319–9323.

20 C. Zhou, J. Han and R. Guo, *Macromolecules*, 2008, **41**, 6473–6479.

21 M. Yang, Z. Xiang and G. Wang, *J. Colloid Interf. Sci.*, 2012, **367**, 49–54.

22 M. J. Kim, Y. D. Liu and H. J. Choi, *Chem. Eng. J.*, 2014, **235**, 186–190.

23 W. Chen, R. B. Rakhi, M. N. Hedhili and H. N. Alshareef, *J. Mater. Chem. A*, 2014, **2**, 5236–5243.

24 J. Sun and H. Bi, *Appl. Surf. Sci.*, 2012, **258**, 4276–4282.

25 W. Chen, R. B. Rakhi and H. N. Alshareef, *J. Phys. Chem. C*, 2013, **117**, 15009–15019.

26 M. M. Sk, C. Y. Yue and R. K. Jena, *RSC Adv.*, 2014, **4**, 5188–5197.

27 Y. Cao and T. E. Mallouk, *Chem. Mater.*, 2008, **20**, 5260–5265.

28 B. Liang, Z. Qin, J. Zhao, Y. Zhang, Z. Zhou and Y. Lu, *J. Mater. Chem. A,* 2014, **2**, 2129–2135.

29 Y. Wan and D. Zhao, *Chem. Rev.*, 2007, **107**, 2821–2860.

30 A. Caballero, L. Hernán, J. Morales, Z. González, A. J. Sánchez-Herencia and B. Ferrari, *Energy Fuels*, 2013, **27**, 5545–5551.

31 S. Sadasivan, D. Khushalani and S. Mann, *Chem. Mater.*, 2005, **17**, 2765–2770.

32 F. Venditti, R. Angelico, G. Palazzo, G. Colafemmina, A. Ceglie and F. Lopez, *Langmuir*, 2007, **23**, 10063–10068.

33 Y. Ding, X. Liu and R. Guo, *Colloids Surf. A: Physicochem. Eng. Asp.*, 2007, **296**, 8–18.

34 F. Lei, B. Yan, H. H. Chen and J. T. Zhao, *Inorg. Chem.*, 2009, **48**, 7576–7584.

35 M. U. Prathap, B. Thakur, S. N. Sawant and R. Srivastava, *Colloid surf. B*, 2012, **89**, 108–116.

36 B. K. Kuila and M. Stamm, *J. Mater. Chem.,* 2010, **20**, 6086–6094.

37 S. Weng, Z. Lin, L. Chen and J. Zhou, *Electrochim. Acta,* 2010, **55**, 2727–2733.

38 Q. Lu, Q. Zhao, H. Zhang, J. Li, X. Wang and F. Wang, *ACS Macro Lett.,* 2013, **2**, 92–95.

39 H. Guan, L. Z. Fan, H. Zhang and X. Qu, *Electrochim. Acta*, 2010, **56**, 964–968.

40 R. Bleta, C. Machut, B. Léger, É. Monflier and A. Ponchel, *Macromolecules*, 2013, **46**, 5672–5683.

41 J. Geng, J. J. Zhu, D. J. Lu and H. Y. Chen, *Inorg. Chem.*, 2006, **45**, 8403–8407.

42 M. Bláha, M. Varga, J. prokeš, A. Zhigunov and J. Vohlídal, *Eur. Polym. J.,* 2013, **49**, 3904−3911.

43 Q. Wu, Y. Xu, Z. Yao, Liu and A.; Shi, G. *ACS Nano,* 2010, **4**, 1963−1970.

44 H. W. Park, T. Kim, J. Huh, M. Kang, J. E. Lee and H. Yoon, *ACS Nano*, 2012, **6**, 7624–7633.

45 B. K. Kuila, B. Nandan, M. Böhme, A. Janke and M. Stamm, *Chem. Commun.*, 2009, **38**, 5749–5751.

46 D. S. Dhawale, R.R. Salunkhe, V. S. Jamadade, D. P. Dubal, S. M. Pawar and C. D. Lokhande, *Curr. Appl. Phys.,* 2010, **10**, 904–909.

47 Y. G. Wang, H. Q. Li and Y. Y. Xia, *Adv. Mater.,* 2006, **18**, 2619–2623.

48 F. Huang and D. Chen, *Energy Environ. Sci.,* 2012, **5**, 5833–5841.

List of Figures

Figure 1 TEM images of PANI synthesized in (a) reverse microemulsion system in the presence of P123, (b) reverse microemulsion system in the presence of CTAB, and (c) traditional microemulsion system in the presence of P123.

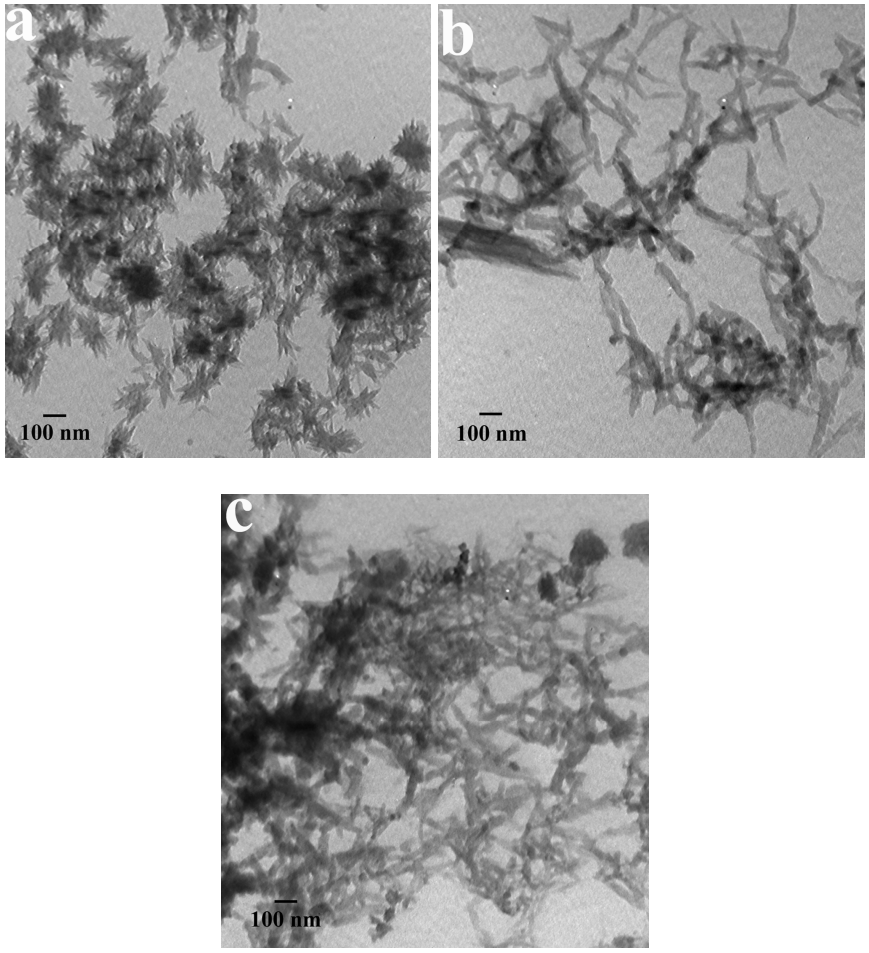

Figure 2 TEM images of PANI prepared in reverse microemulsion system with different concentrations of P123. (a) [P123] = 0 M; (b) [P123] = 0.002 M; (c) [P123] = 0.006 M; (d) [P123] = 0.011 M. The concentration of AN is 0.12 M.

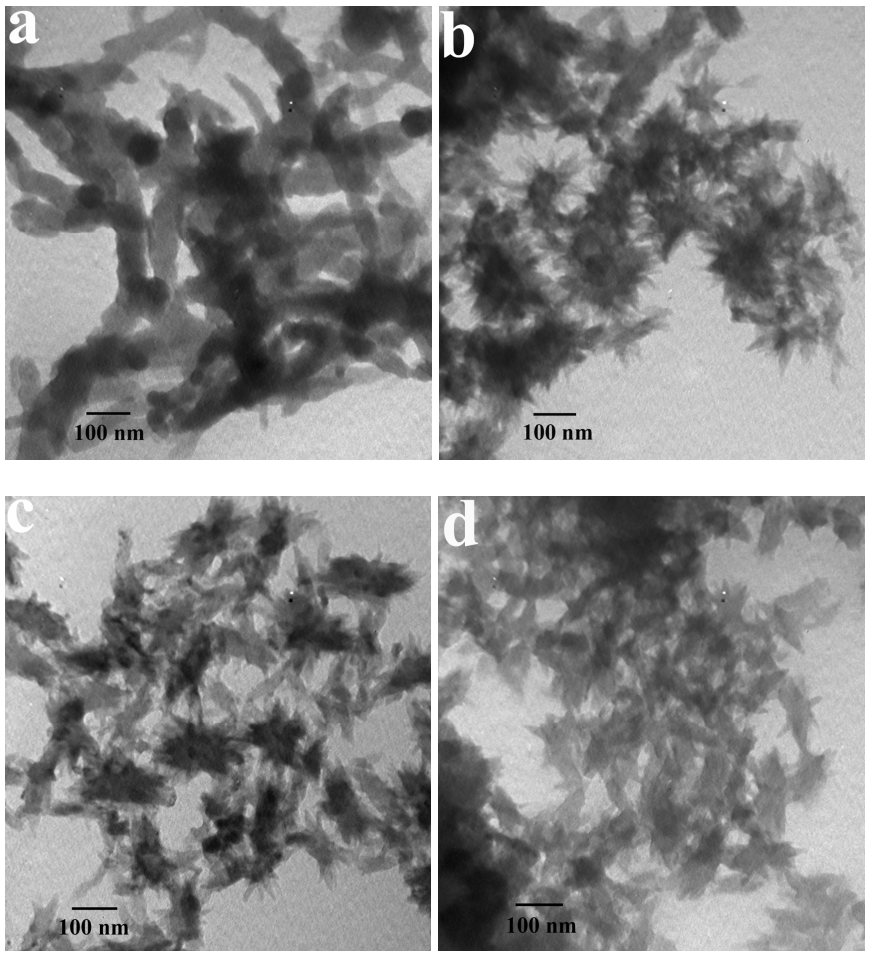

Figure 3 TEM images of PANI with different concentrations of AN. (a) [AN] = 0.07 M; (b) [AN] = 0.17 M. The concentration of P123 is 0.006 M.

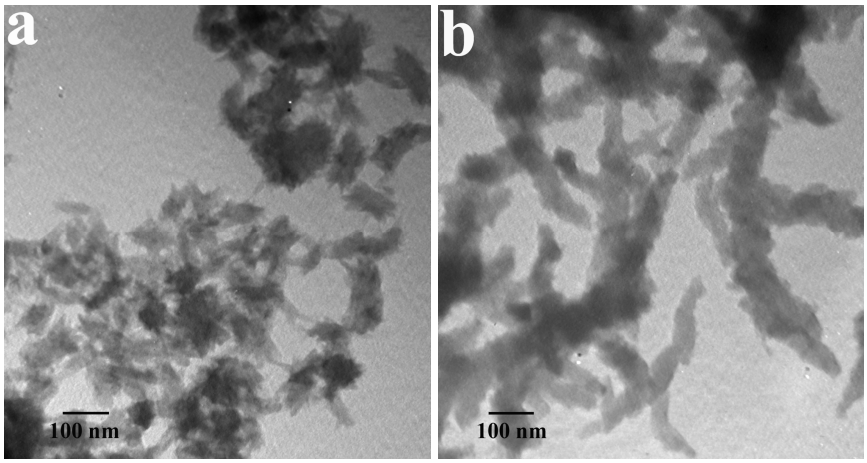

Figure 4 TEM images of PANI obtained from various reaction stages. (a) 10 min; (b) 30 min; (c) 1 h and (d) 5 h. The concentrations of P123 and AN are 0.006 M and 0.12 M, respectively.

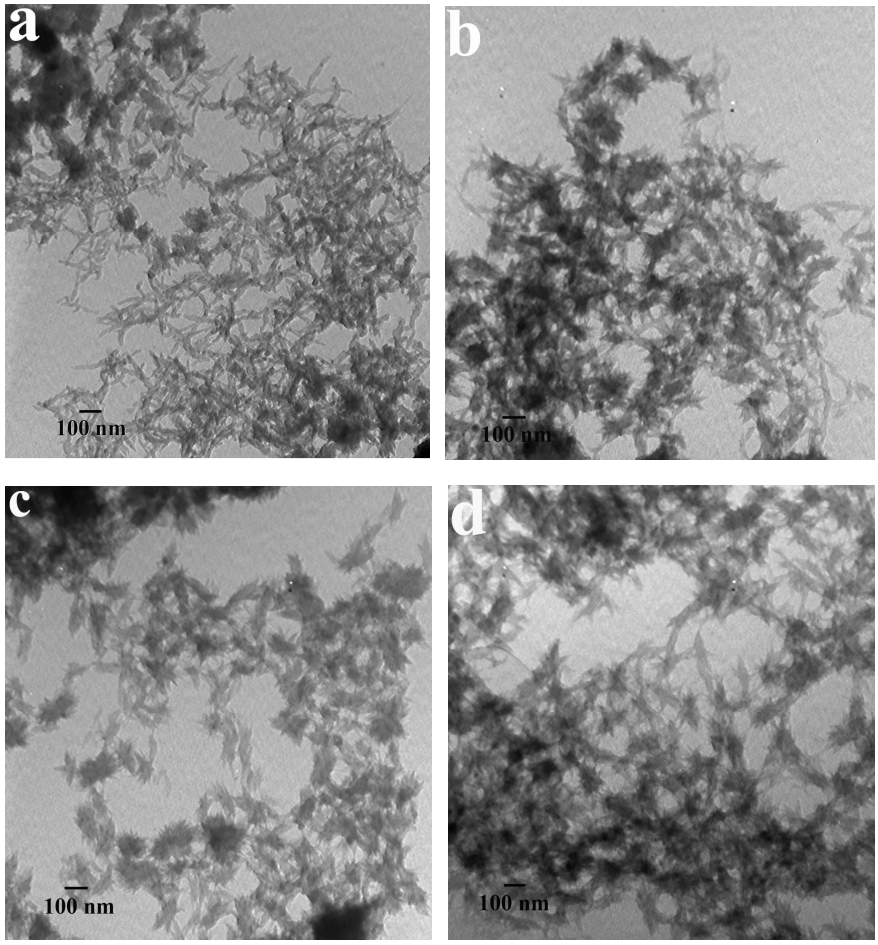

Figure 5 Conformation of P123, and fabrication procedure and possible formation mechanism of PANI nanoflowers.

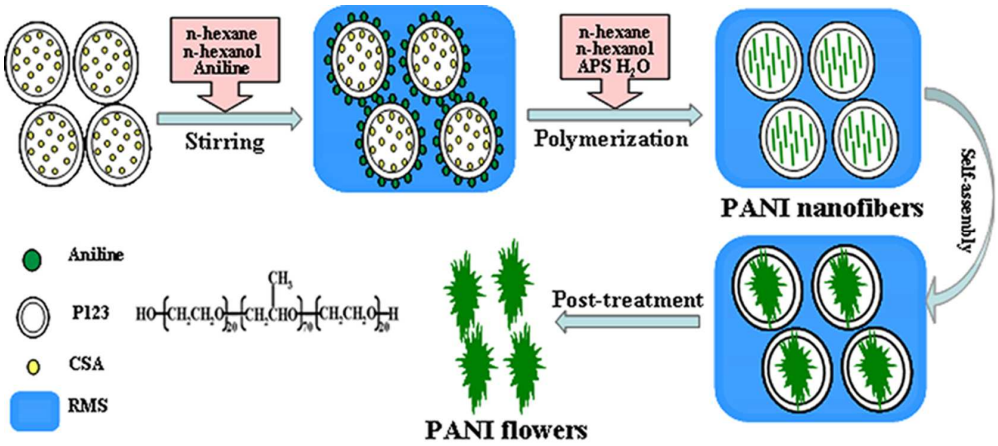

Figure 6 (a) IR spectrum and (b) XRD pattern of PANI nanoflowers. (c) N_2 adsorption−desorption isotherms of PANI nanoflowers.

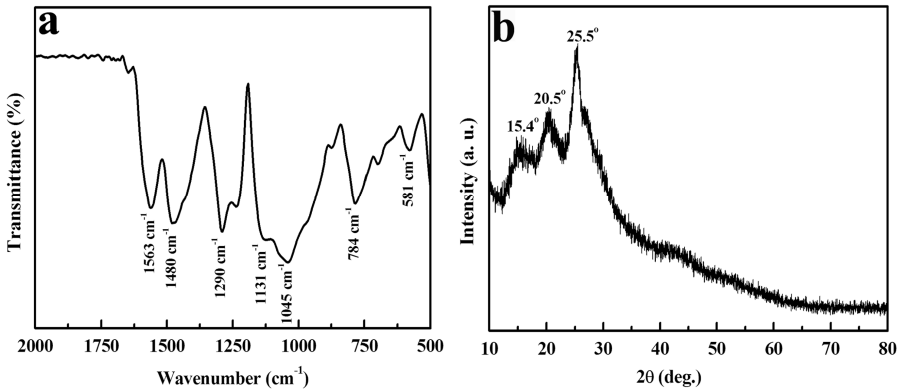

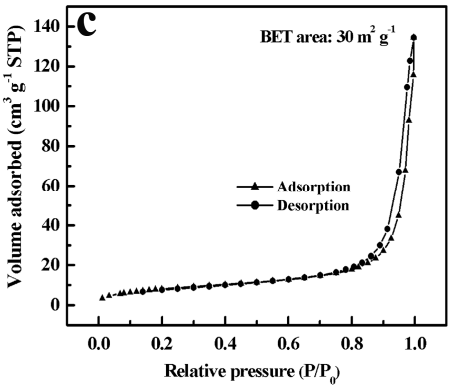

Figure 7 Electrochemical performance of PANI electrodes in 1 M H_2SO_4 electrolyte. (a,b) CV curves of (a) PANI nanoflowers and (b) PANI nanofibers at various scan rates of 1, 3, 5, 7 and 9 mV s^{-1}. (c,d) Galvanostatic CD curves of (c) PANI nanoflowers and (d) PANI nanofibers at various current densities of 0.5, 1, 1.5 and 2.0 A g^{-1}. The inset is the plots of charge/discharge capacitance versus current density. (e) Cycling performance at a current density of 5 A g^{-1}. (f) Nyquist plots of PANI nanoflowers and PANI nanofibers. The inset shows the magnified plots in high frequency region.